Extreme Precipitation and Atmospheric Rivers in a Model of Pliocene Climate

Sofia Menemenlis

Advisor: Juan Lora

Second Reader: Alexey Fedorov

29 April 2020

A Senior Thesis presented to the faculty of the Department of Geology and Geophysics, Yale University, in partial fulfillment of the Bachelor's Degree.

Abstract

While it is understood that overall precipitation will increase as the climate warms, our knowledge of how warmer temperatures will affect the intensity, frequency, and regional distribution of the heaviest precipitation events is less established. The mid-Pliocene warm period (mPWP), or mid-Piacenzian, is an example of a warm past climate with concentrations of atmospheric CO_2 comparable to those of the present. It is often invoked as a possible analog for the long-term effects of climate change. This study analyzes output from one model of mid-Piacenzian climate—the University of Toronto Version of the Community Climate System Model Version 4 (UofT-CCSM4)—to examine changes in patterns of extreme precipitation in the Pliocene. It focuses on midlatitude regions where atmospheric rivers (ARs) play a major role in transporting water vapor, and uses vertically-integrated vapor transport anomalies to identify changes in AR behavior. Globally, there is an overall increase in the intensity and frequency of the heaviest precipitation events in the Pliocene simulation, particularly of the very heaviest events. Regionally, changes in the hydrologic cycle are influenced by a combination of thermodynamic and dynamic factors. Two strongly AR-influenced areas—the Pacific coast of North America and the Pacific coast of Chile—experience distinctly different patterns of change in extreme precipitation. These differences can largely be explained by changes in AR behavior in the Pliocene simulation, highlighting the effects of ARs on regional patterns of precipitation. This study also has implications for the design of future experiments using Pliocene climate models, and for further efforts to better constrain Pliocene conditions using proxy data.

Contents

1. Introduction

Anthropogenic climate change takes place on a planetary scale, but impacts communities and landscapes in uneven, "patchy" ways (Tsing et al. 2019). Changes in patterns of extreme weather events are among the most disruptive impacts of climate change, and constitute a broad phenomenon whose impacts on particular landscapes vary dramatically. As the planet warms, higher atmospheric water vapor content will drive increases in overall precipitation and in the intensity of the heaviest events (Held and Soden, 2006). Models of 21st-century climate simulate increases in extreme precipitation—events exceeding a certain high percentile of daily precipitation—in most parts of the world, even as mean precipitation increases in some areas and decreases in others (O'Gorman and Schneider, 2009). However, the science of how such changes in intensity will occur, how the frequency of extreme events will change, and where these changes will occur is still evolving. The Fifth Assessment Report (AR5) of the Intergovernmental Panel on Climate Change stated that heavy precipitation events had *likely* increased in more regions than they had decreased (IPCC, 2013). Although there have been advancements in our knowledge since the publication of AR5, significant gaps remain (Alexander, 2016).

The mid-Piacenzian warm period (referred to also as the mid-Pliocene Warm Period) lasted from 3.264 – 3.025 Ma. It represents a warm interval of the Pliocene epoch that, to the extent it can be seen as analogous to a future warmer climate, may help to predict impacts of anthropogenic warming. The mid-Piacenzian is the most recent time in Earth's history that global temperatures exceeded those of the present for a span of time longer than any of the Pleistocene interglacial periods (Haywood et al. 2016). And while primary forcings of the warm Pleistocene interglacial periods were increases in northern hemisphere summer insolation, the warmer-than-present conditions of the mid-Piacenzian were likely due to elevated pCO_2 (Chandan & Peltier, 2018; Martínez-Botí et al., 2015). CO_2 levels at the time are estimated to have fallen between 350–450 ppmv, a range that encompasses present-day concentrations (e.g. Pagani et al., 2009; Bartoli et. al., 2011; Badger et al., 2013). Mid-Piacenzian continental configuration, land elevation, and ocean bathymetry were relatively similar to those of the present. The sustained period of warmth during the mid-Piacenzian would have allowed Earth's climate system to equilibrate to increased temperatures, demonstrating the effects of such warming on longer time-scales (Haywood et al., 2016).

Numerical climate modeling and proxy-based environmental reconstructions of the mid-Piacenzian contribute to our understanding of Earth-system climate sensitivity (ESS), defined as the increase in global temperature in response to a doubling of pCO_2, incorporating long-term feedbacks such as changes in ice sheets. Previous studies of mid-Piacenzian climate have suggested that ESS exceeds climate sensitivity (CS), by approximately 50% (Haywood et al., 2013; Haywood et al., in review).

The mid-Piacenzian may also contribute to our understanding of dynamic effects of climate change. Pliocene warming was accompanied by an amplification of polar warming and a weakening of the meridional temperature gradient (Haywood et al., 2016). The tropical Hadley and Walker circulations were weaker than in the preindustrial (Corvec and Fletcher, 2017), as they are also projected to be with future climate change (e.g., Vecchi and Soden, 2006; Vallis et al., 2014). Proxy estimates place global mean sea level at approximately 20 meters above that of the present-day due to substantial ice loss in both hemispheres, although these estimates still carry considerable uncertainty (Dutton et al., 2015; Grant et al., 2019). A combination of model results and paleobotanical data reveal a generally wetter mid-Piacenzian climate, accompanied by the expansion of forests, tropical savannas, and woodlands, and by a contraction of deserts (Salzmann et al., 2008).

The ability of paleoclimate models to reproduce broad features of the mid-Piacenzian has improved (Haywood et al. 2013, Haywood et al. in review). If models of the mid-Piacenzian can reproduce changes in the hydrologic cycle caused by elevated CO_2 forcing, they then offer a particularly useful way to learn about extreme precipitation in a warmer world, especially because relatively short observational records provide limited information about changes in extreme events on longer timescales. This study explores this vein of analysis using one model of Pliocene climate.

2. Methods

I analyze output from simulations generated by the University of Toronto version of the Community Climate System Model Version 4 (UofT-CCSM4), which is described in Chandan & Peltier (2017). This model was developed under the framework of the Pliocene Model Intercomparison Project Version 2 (PlioMIP2), an international collaboration to quantify uncertainties in and improve upon models of Pliocene climate (Haywood et al. 2016). PlioMIP2

builds upon the previous efforts of PlioMIP1, using fifteen different climate models which vary in spatial resolution and levels of complexity (Haywood et al., in review). It focuses on the more specific temporal window of 3.264–3.025 Ma, during which astronomical parameters were similar to present-day values (Haywood et al., 2016).

PlioMIP2 models use as boundary conditions the paleoenvironmental reconstructions contained in the Pliocene Research, Interpretation, and Synoptic Mapping Version 4 (PRISM4) dataset. Improving upon earlier versions of PRISM reconstructions, it represents our best current understanding of mid-Piacenzian conditions. PRISM4 includes reconstructions of topography/bathymetry, biomes, soils, lakes, ice sheets, and sea surface temperature (Dowsett et al. 2016). Sea surface temperature reconstructions are used for data-model comparison. Two particularly significant PRISM4 updates to the PRISM3 dataset, which was used for PlioMIP1 experiments, are closed Arctic ocean gateways and a reduced pole-to-equator temperature gradient. See Dowsett et al. (2016) for further information about the PRISM4 dataset, and Haywood et al. (2016) for further information about PlioMIP2 experimental design.

The UofT-CCSM4 is modified from the original NCAR CCSM4 to attempt a more faithful reproduction of the Pliocene climate (Chandan and Peltier, 2017). It includes a modified ocean component of the NCAR CCSM4 to remove the overflow parametrization and tidal mixing schemes, which were deemed to be highly tuned to modern-day conditions (Chandan and Peltier, 2017. It also fixes the vertical profile of diapycnal diffusivity to that which was used in the ocean component (POP1) of the CCSM3 model. Using the "enhanced" version of the PRISM4 boundary conditions, the UofT-CCSM4 achieves a better match between simulated climatology and proxy-based reconstructions than with the PRISM3 dataset (Chandan and Peltier, 2017). In particular, it simulates elevated high-latitude warming and more than double the global mean temperature increase as with earlier boundary conditions (Chandan and Peltier, 2017). The simulated mid-Piacenzian climate is 3.8°C higher than the preindustrial control, and 1.8°C higher than the modern control. This level of mid-Piacenzian warming falls close to the upper end of estimates produced by PlioMIP2 models (Haywood et al., in review). The UofT-CCSM4 also displays increased seasonal temperature differences in the Pliocene simulation, showing an amplification of average surface warming in the Northern Hemisphere summer (Chandan and Peltier, 2017).

In my analysis, I compare the results of the UofT-CCSM4 mid-Piacenzian experiment to the results of two other simulations, meant to reproduce conditions of a preindustrial and a "modern" climate. The mid-Piacenzian simulation, Eoi400, incorporates all PRISM4 boundary conditions and sets pCO_2 at 400 ppmv. The preindustrial control, E280, uses preindustrial boundary conditions and sets CO_2 at 280 ppmv. The modern simulation, E400, uses the same boundary conditions as in the preindustrial simulation, but sets CO_2 at 400 ppmv. So as to eliminate ambiguities introduced by changing orbital parameters, all three simulations share a solar constant S_0 of 1365 Wm^{-2}, eccentricity $e = 0.01624$, obliquity $\varepsilon = 23.446°$, and the longitude of perihelion $\omega = 102.04°$. The simulations use a finite volume grid with 192 cells in latitude, 288 cells in longitude, and 26 vertical levels. It is important to note that each simulation is run to near statistical equilibrium, although Chandan and Peltier (2017) note that the deep ocean continues to warm, as it takes much longer than the atmosphere or sea surface temperatures to reach equilibrium. More details about the specific configurations of each simulation are presented by Chandan and Peltier (2018). In this paper I will refer to the E280, E400, and Eoi400 simulations as the preindustrial, modern, and Pliocene simulations respectively.

Because the Pliocene simulation incorporates updated boundary conditions that are not present in the modern or preindustrial, we expect the simulated Pliocene climate to respond to forcings that do not affect the modern or preindustrial climates. Some forcings can be attributed to conditions particular to the Pliocene, for example in topography changes or the land-sea mask, and can help identify which features of the Pliocene climate may be considered analogs to features we might expect in a warmer future climate. Chandan and Peltier (2018) used a factorization technique to compare the effects of three out of the four types of boundary conditions that most affect mid-Pliocene climate: orography, ice sheet configuration, and change in pCO_2 (the fourth factor, ocean bathymetry, was not analyzed and was held constant in each simulation). They found that the change in pCO_2 was the most significant contributor to global mean temperature increase in the Pliocene model.

For each simulation, I work with 20 years of daily data for several variables. To calculate sea surface temperature, I average temperatures over the atmospheric level closest to the surface of the Earth. Note that Chandan and Peltier (2017) compute surface air temperature anomalies using 2 m air temperature, resulting in minor differences in calculated absolute values of mean

surface temperature, although the magnitude of changes between simulations remains constant. To calculate total precipitation, I take the sum of convective and large-scale precipitation. To calculate precipitation minus evaporation (*P–E*), I subtract surface moisture flux from total precipitation.

In order to analyze changes in the heaviest precipitation events, I define extreme precipitation as those daily precipitation values that exceed the value of a certain percentile of preindustrial precipitation. I calculate the frequency of precipitation extremes simply by adding together the number of daily precipitation events in a given location that exceed said value, and report the result as a percentage of total days. To illustrate, for a given set of longitude, latitude coordinates, the following would give the percentage of extreme precipitation days:

$$\frac{number\ of\ days\ with\ precipitation\ exceeding\ preindustrial\ 99th\ percentile}{total\ number\ of\ days} \times 100$$

One limitation to note is that this method measures extreme precipitation frequencies as independent values for each grid point, and therefore does not fully account for correlation between precipitation values in the same area.

This analysis will also use daily precipitation data to examine the role of atmospheric rivers (ARs) in moisture transport and heavy precipitation. ARs are narrow corridors of moisture in the atmosphere that account for most poleward moisture transport outside of the tropics (Zhu and Newell, 1998). They are associated with extreme storms, especially when they encounter topographical features, and are therefore important to the distribution of heavy precipitation events in the midlatitudes. In recent years, ARs have emerged as a growing topic of research (Ralph et al., 2017). They have been studied most extensively in relation to the west coast of North America (e.g., Payne and Magnusdottir, 2014; Rutz et al., 2013). However, they are similarly important in other parts of the world, for example the west coast of South America (Viale et al., 2018). This study uses a method that identifies ARs based on vertically integrated vapor transport (IVT) exceeding a latitudinally-dependent threshold that depends on integrated water vapor, which enables comparisons across climates (Skinner et al., accepted) . A similar version of this method has been applied to study atmospheric rivers during the Last Glacial Maximum (Lora et al. 2017). Lora et al. (2017) note that this method likely underestimates AR

precipitation over land, because atmospheric rivers may persist even as they become too small to detect.

In this study, I analyze global trends in the hydrologic cycle. Then, I focus more specifically on extratropical precipitation and precipitation extremes, where ARs play an important role in moisture transport. In the midlatitudes, precipitation patterns are controlled to a great extent by large-scale atmospheric processes (O'Gorman and Schneider, 2009), meaning that dynamical changes in ocean and atmospheric circulation significantly affect how precipitation patterns change in a warmer climate. In general, simulations of extratropical precipitation are fairly consistent both across different models and in comparison to paleoclimate proxies (Haywood et al., 2013; Dowsett et al., 2016). Uncertainty in model reproductions of tropical precipitation is significantly larger, in part because overall precipitation in the tropics is substantially greater.

3. Global Patterns of Change

Figure 1 shows how surface temperature, precipitation, and precipitation minus evaporation ($P–E$) changed between the modern and preindustrial, Pliocene and preindustrial, and Pliocene and modern simulations. Annual mean surface temperature in the Pliocene control is 289.7 K, compared to 285.9 K in the preindustrial and 287.9 K in the modern. Average surface temperature in the Pliocene simulation is thus 3.8 K greater than in the preindustrial. The Pliocene experiment reproduces the amplified high-latitude warming that is a key feature of mid-Piacenzian proxy reconstructions (Figure 1b), highlighting the role of negative ice-albedo and possibly cloud-albedo feedbacks at high latitudes. The mid-Piacenzian flattening of the meridional temperature gradient directly affects atmospheric pressure systems, the behavior of the Hadley circulation, and the position of westerly wind belts (Haywood et al. 2016). The importance of these features for the hydrologic cycle will be explored later in this paper. While this paper focuses more attention on the effects of weaker meridional temperature gradients, the effects of the concurrent weakening of zonal temperature gradients is an important ongoing area of study (e.g., Wara et al., 2005; O'Brien et al., 2014; Fedorov et al., 2010).

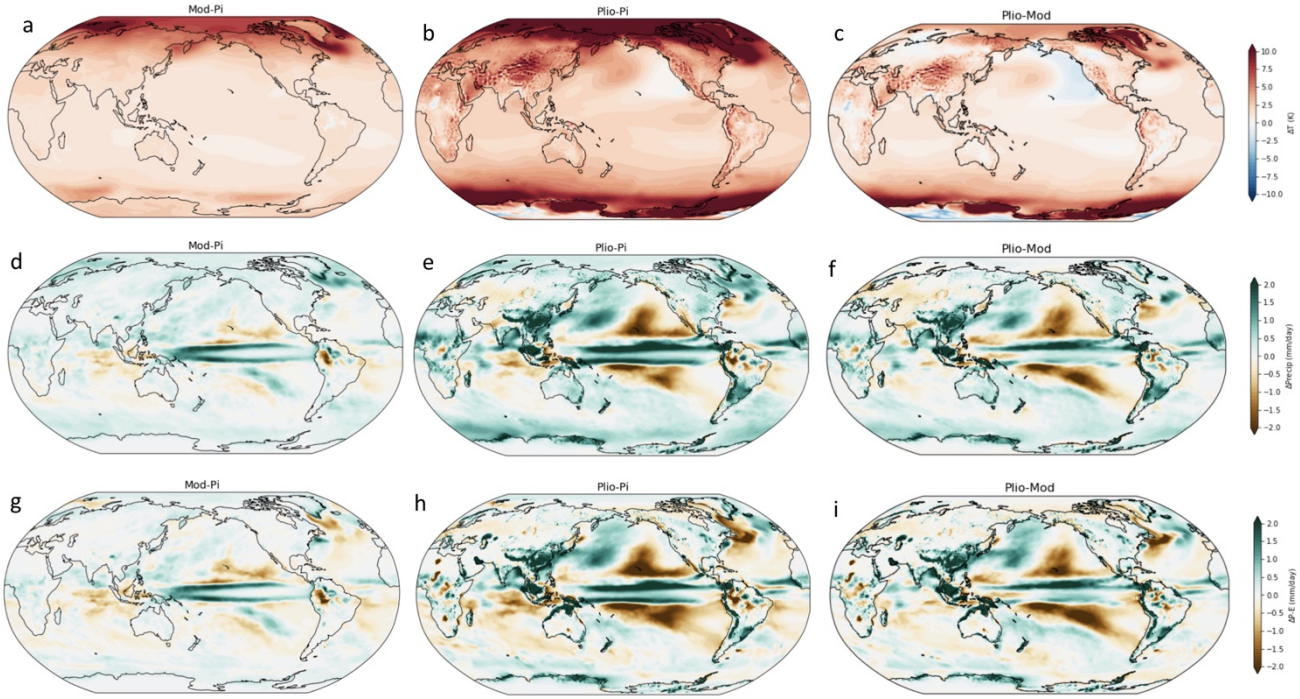

Figure 1. *(a–c) Differences in annual mean surface temperature, in °K, between the modern and preindustrial (a), Pliocene and preindustrial (b), and Pliocene and modern (c) simulations respectively. (d–f) Differences in annual mean precipitation, in mm/day, between the modern and preindustrial (d), Pliocene and preindustrial (e), and Pliocene and modern simulations (f). (g–i) Differences in annual mean precipitation – evaporation between the modern and preindustrial (g), Pliocene and preindustrial (h), and Pliocene and modern (i) simulations.*

Changes in the hydrologic cycle can be attributed to a combination of thermodynamic and dynamic elements. The Clausius-Clapeyron relation describes how, at typical lower troposphere temperatures, saturation vapor pressure increases by approximately 7% per K of warming (Held & Soden 2006). This is the basic thermodynamic explanation of precipitation increases in warmer climates. In both the modern (figure 1g) and Pliocene (figure 1h) simulations, the hydrologic cycle intensifies particularly in areas that already receive higher levels of precipitation. This can be explained by the "wet gets wetter, dry gets drier" response of *P–E* as, assuming no major changes in atmospheric circulation, increased column water vapor converges in already-wet areas. The effect is most obvious over the oceans where evaporation is

not limited by surface moisture, and is robustly predicted in projections of future climate change (Held & Soden, 2006; Trenberth, 2011).

In the UofT-CCSM4 model, global mean precipitation increases by 0.22 mm/day compared to the preindustrial, and by 0.11 mm/day in the modern. A roughly 2% increase in overall precipitation per K of warming, for both the modern and Pliocene simulations, is much lower than Clausius-Clapeyron scaling. This can be attributed to the fact that as lower-tropospheric water vapor increases, mass exchange between the boundary layer and mid-troposphere decreases, resulting in a slower overall atmospheric circulation (Held and Soden 2006).

Changes in dynamic aspects of atmospheric circulation affect the hydrologic cycle alongside thermodynamic changes (Seager et al., 2010). Shifts in atmospheric circulation can be related to reduced meridional near-surface temperature gradients, which generate a broadening and weakening of the Hadley circulation in the Pliocene climate (Haywood et al., 2016). This type of dynamic change can substantially alter precipitation anomalies, particularly within convergence zones (Chou et al., 2009). Burls and Fedorov (2017) used the weakening of meridional sea surface temperature gradients to explain proxy evidence that suggests savannas and woodlands existed during the Pliocene in presently arid subtropical regions of Africa and Australia. They demonstrated how a weaker meridional circulation could have decreased moisture divergence and contributed to a generally wetter climate in subtropical regions, which can be observed in figure 1. Similarly, Li et al. (2015) analyzed PlioMIP simulations to demonstrate how a poleward shift of mean meridional circulation would have contributed to a poleward shift of midlatitude westerly winds. As Seager et al. (2010) described, the behavior of transient eddies, which bring moisture from the subtropics to higher latitudes, evolves in ways that can only partially be explained by thermodynamic mechanisms. These dynamics will be discussed further in the context of the UofT-CCSM4 model in the later section of this paper.

Some of the evident shifts in precipitation patterns can be attributed to boundary conditions that are specific to the PRISM4 mid-Piacenzian reconstruction. Higher elevations in regions such as the Himalayas, Tibetan Plateau, and Andes, combined with the higher moisture content of rising air in those areas, result in significant precipitation increases in the Pliocene simulation as compared to the preindustrial or modern. The increases in precipitation evident in

the northern part of the Australian continent can be attributed to the Sahul and Sunda shelves, which are subaerial in PRISM4 boundary conditions (Dowsett et al. 2016).

Observations, models, and theory concur that as the hydrologic cycle intensifies in a warming climate, more extreme precipitation events occur (e.g., Min et al. 2011; Zhang et al. 2013; Donat et al. 2016; Fischer and Knutti 2016). However, heavy rainfall responds differently to warming than does mean annual precipitation (Fischer and Knutti 2016). Katz and Brown (1992) explain using statistical theory how the frequency of extreme values of a given climate variable is relatively more dependent on changes in the variability than the mean of that variable. The relative sensitivity of an extreme event to the scale parameter σ becomes proportionately greater than its relative sensitivity to the location parameter μ as the even becomes more extreme. Myhre et al. (2019) demonstrate this effect using climate models and observations from recent decades, documenting clear increases in the intensity and frequency of extreme precipitation with event rareness as the climate warms.

Figure 2 depicts changes in patterns of extreme precipitation for the modern and Pliocene simulations. Figure 2a documents changes in the intensity of the heaviest precipitation events. Data from the preindustrial, modern, and Pliocene simulations show that the intensity of extreme precipitation events increase monotonically with temperature, whether an extreme event is defined as the 99^{th}, 99.9^{th}, or 99.97^{th} percentile of daily precipitation values. Moreover, figure 2b shows that the rate of increase of the intensity of extreme precipitation events more than doubles in the Pliocene warming scenario compared to the modern warming scenario.

Figure 2c shows changes in the frequency of extreme precipitation events. The frequency of extreme events has been defined as the percent of daily precipitation events exceeding the value of a certain percentile (99^{th}, 99.9^{th}, or 99.97^{th}) of daily precipitation events in the preindustrial control. These values were calculated at each model grid point, and their global mean values were plotted. Like intensity, the frequency of precipitation extremes increases monotonically with global mean surface temperature, to substantial effect. Ignoring regional differences, the average approximately once-per-decade (99.97^{th} percentile) preindustrial daily precipitation event would occur two or three times per decade in the modern simulation, and six or seven times per decade in the Pliocene control. Figure 2d compares rates of increase in the Pliocene and modern control. Rates of increase in the frequency of extremes substantially exceed rates of increase in the intensity of extremes. Myhre et al. (2019) show that changes in

total extreme precipitation are dominated by increases in the frequency of extreme precipitation, although changes in intensity of extremes are still important. Figure 2d suggests that not only does this pattern hold true in the modern, it also intensifies in the Pliocene.

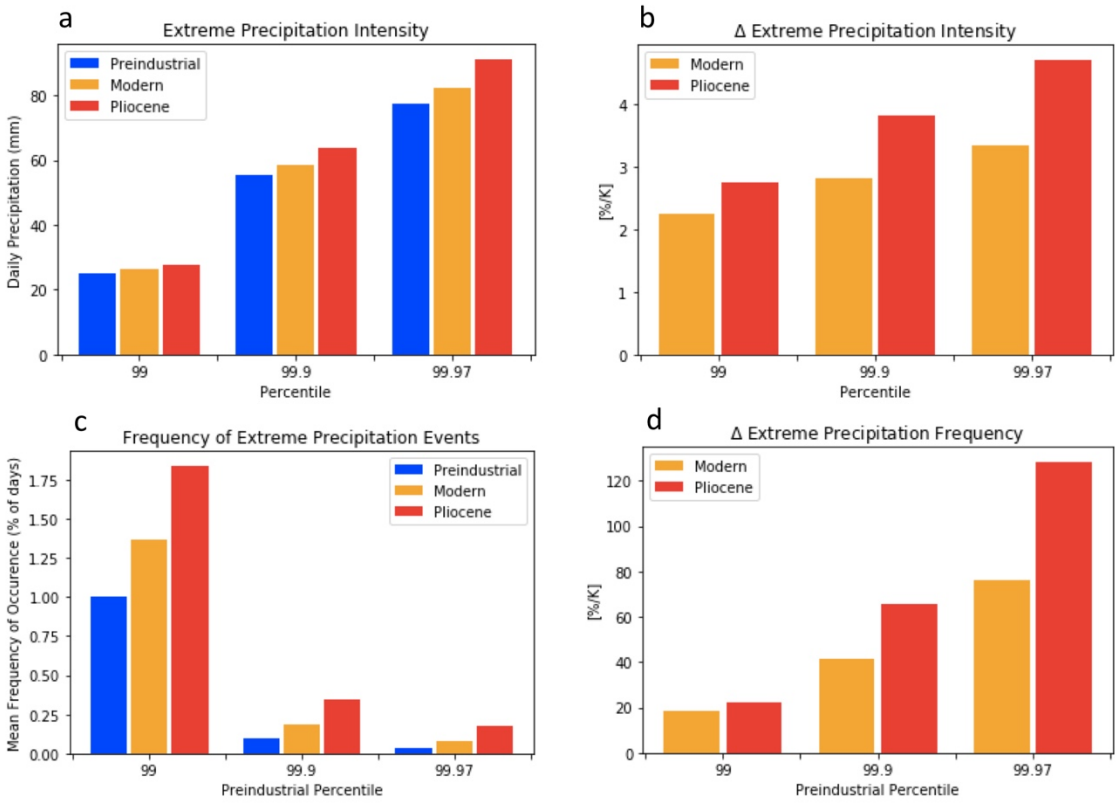

Figure 2. *(a) Magnitudes of high percentiles of extreme daily precipitation for the preindustrial, modern, and Pliocene. (b) Rates of change from the preindustrial values of the values shown in (a) for the modern and Pliocene, expressed as % change per K. (c) Frequency of precipitation events exceeding the 99th percentile of daily precipitation in the preindustrial simulation, expressed as % of days. Note that because precipitation extremes are defined based on the preindustrial control, the frequency of extreme precipitation in the preindustrial is 1% for events exceeding the 99th percentile, etc., and is shown for reference. (d) Rates of change from the preindustrial for the values shown in (c), for the modern and Pliocene, expressed as % change per K.*

The behavior of extremes as the climate warms is in general agreement with statistical theory as described in Katz et al. (2012), and exemplifies the same broad patterns as observations and model simulations of present-day and short-term future warming. It is unclear to what extent

the substantially increasing rates of change in the Pliocene as compared to the modern, as depicted in figures 2b and 2d, would be reproduced in other models of future and past warming scenarios. However, given the significance of these increases, this would be an interesting area for future study.

The globally averaged values in figure 2 disguise large differences in regional effects. Not only does heavy precipitation respond differently to warming than overall rainfall, but the spatial distribution of changes in extreme precipitation is heterogeneous, with sometimes opposite effects in different locations (Fischer and Knutti, 2016; Donat et al., 2016). Like changes in mean precipitation, this is due to a combination of dynamic and thermodynamic effects. Particularly in the extratropics, where the atmosphere is in general more stable, no simple thermodynamic explanation can account for patterns of extreme precipitation. Extreme precipitation events do not scale with mean atmospheric water vapor content, or with mean moisture convergence at the base of storms (O'Gorman and Schneider, 2009).

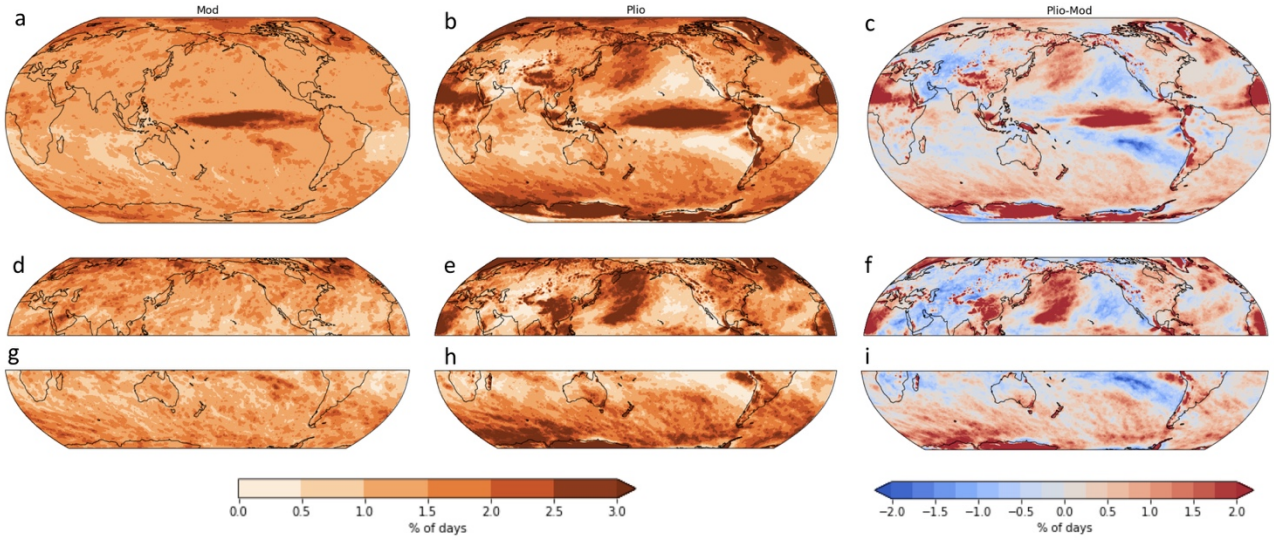

Figure 3. *(a–b) Frequency of events exceeding the 99th percentile of preindustrial precipitation at each grid point (% of days), for the modern (a) and Pliocene (b). (c) Difference between (b) and (a). (d–e) Frequency of NH cool-season (November–April) precipitation exceeding 99th percentile of preindustrial NH cool-season precipitation. (f) Difference between (e) and (d). (g–h) Frequency of SH cool-season (May–October) precipitation exceeding 99th percentile of SH cool-season precipitation. (i) Difference between (h) and (g).*

Figures 3a–c show changes in the frequency of precipitation exceeding the 99th percentile of the preindustrial control precipitation at each grid point. In the midlatitudes, where ARs play a key role in the water cycle, changes in extreme precipitation frequency are highly variable and are dominated by signals most evident in the cool seasons of either hemisphere, e.g., November–April in the northern hemisphere and May–October in the southern hemisphere. Figures 3d–f depict changes in the frequency of extremes for the northern hemisphere cool season, while figures 3g–i depict changes in the frequency of extremes for the southern hemisphere cool season.

4. Regional Influence of Atmospheric Rivers

Occupying a mere 10% of available longitude, atmospheric rivers are responsible for approximately 90% of poleward water vapor transport in the extratropics (Zhu and Newell, 1998). They lead to heavy precipitation over certain areas on land, particularly when they encounter topographical barriers such as the Sierra Nevada or Andes mountains (Rutz et al., 2013). Their role in transporting water vapor from over the ocean is an important reason why precipitation extremes over land may not scale with local mean surface temperature (O'Gorman 2015). With future warming, changes in atmospheric circulation and synoptic-scale weather systems may affect ARs in ways that are not yet understood.

I focus my analysis on AR behavior as it affects two regions over land, western North America and the central/southern coast of Chile, where ARs are known to play a major role in the regional hydrologic cycle (e.g., Rutz et al., 2013; Payne and Magnusdottir, 2014; Viale and Nuñez, 2010; Viale et al., 2018). These are by no means the only areas where dynamical changes in AR behavior contribute to significant changes in precipitation extremes. Europe and Japan, for example, stand out as areas of interest based on patterns of AR behavior and changes in extreme precipitation evident in the UofT-CCSM4 Pliocene model experiments. Moreover, ARs have been shown to have important cool-season influence on the hydrologic cycle in areas like Britain and South Africa (Lavers et al., 2013; Blamey et al, 2017). Nevertheless, the Pacific coasts of extratropical North America and South America demonstrate the significance of regional changes in midlatitude extreme precipitation in the context of changing AR behavior.

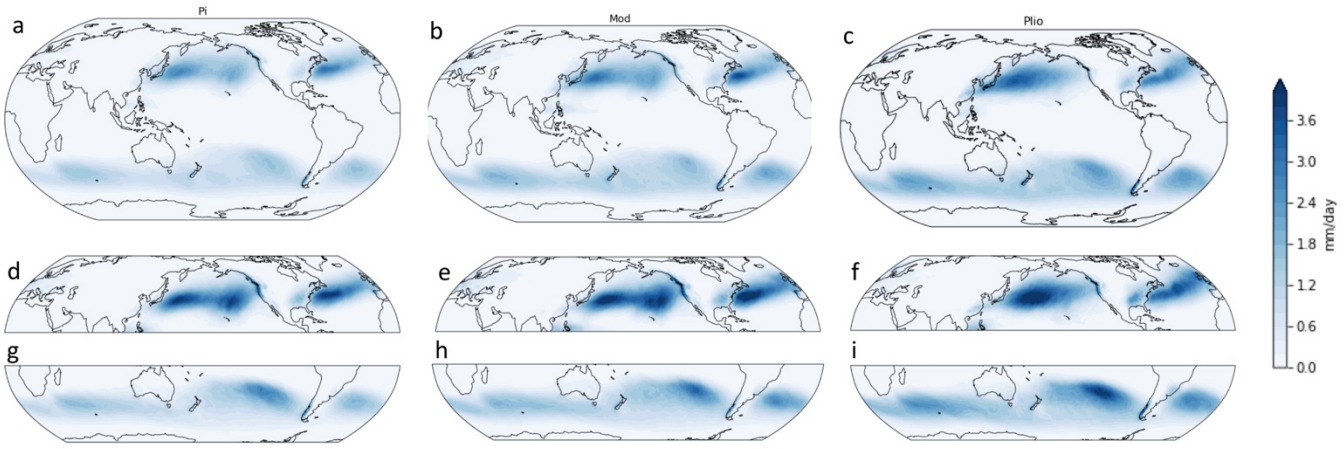

Figure 4. *(a–c) Mean AR precipitation (mm/day), based on the co-occurrence of atmospheric rivers and precipitation events, for the preindustrial (a), modern (b), and Pliocene (c). (d–e) Mean AR precipitation in the NH cool season (November–April) for the preindustrial (d), modern (e), and Pliocene (f). (g–i) Mean AR precipitation in the SH cool season (May–October) for the preindustrial (g), modern (h), and Pliocene (i).*

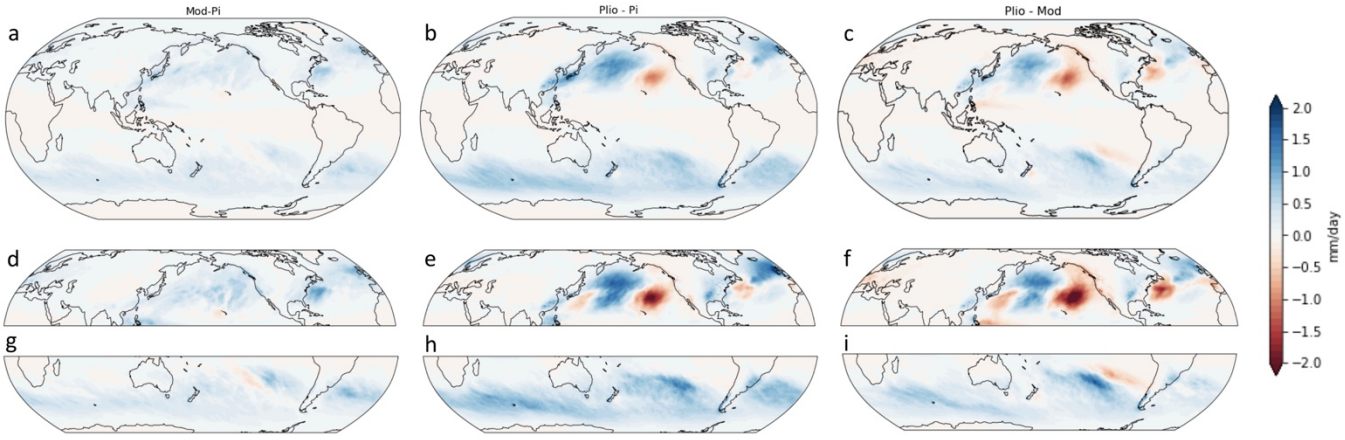

Figure 5. *(a–c) Changes in mean AR precipitation (mm/day) between the modern and preindustrial (a), Pliocene and preindustrial (b), and Pliocene and modern (c). (d–e) Changes in mean AR precipitation in the NH cool season (November–April) between the modern and preindustrial (d), Pliocene and preindustrial (e), and Pliocene and modern (f). (g–i) Changes in mean AR precipitation in the SH cool season (May–October) between the modern and preindustrial (g), Pliocene and preindustrial (h), and Pliocene and modern (i).*

Figure 4 displays mean AR precipitation, while figure 5 displays changes in mean AR precipitation. Like changes in extremes, the annual mean is dominated by changes in AR precipitation during the cool-season months of each hemisphere, when extratropical cyclones are more prevalent. In each respective cool season, figure 4d–i and figure 5d–i reveal changes in patterns of Pliocene AR precipitation that are distinctly different from the modern.

In the north Pacific, AR behavior shifts northwest. This results in an increase in AR precipitation over the northwestern parts of the north Pacific, and a decrease in AR precipitation over eastern parts of the north Pacific and over the adjacent north American coast (figure 5e). The mechanisms for this shift in AR behavior appear related to a number of factors. In the cool season, the Aleutian low strongly influences the trajectory of the extratropical cyclones that influence AR formation. While in the modern simulation the Aleutian low deepens slightly compared to the preindustrial control (figure 6d), in the Pliocene it shrinks significantly and appears to split into two sections (figure 6f for changes, absolute values in appendix 10). This results in sea level pressure anomalies in the cool-season north Pacific that more closely resemble their warm-season configuration, in which the Aleutian low shrinks and shifts northward, ceding its location to the north Pacific high pressure system. This shift may partially explain the decrease in AR activity in the eastern North Pacific.

Figures 6b and 6e reveal increased sea level pressure anomalies in the Pliocene Arctic. These higher sea level pressure anomalies extend into the north Pacific around the location of the Bering Strait. Thus, complicating our interpretation of these changes is the effect of changes in ocean gateways in Pliocene boundary conditions. Ocean gateways have a considerable effect on ocean and atmospheric circulation; for example, Otto-Bleisner et al. (2017) demonstrated the potentially significant impact of the closing of Arctic gateways on the Atlantic meridional overturning circulation and North Atlantic sea surface temperatures. It is not known for certain when the Bering Strait opened, and the timing of its opening would have depended on changes in global sea level (Hu et al. 2010), estimates of which are still highly uncertain for the Pliocene (Dutton et al. 2015). While PRISM3 paleogeography had an open Bering Strait connecting the north Pacific to the Arctic ocean (Dowsett et al. 2012), PRISM4 boundary conditions have both the Bering Strait and the Canadian Arctic Archipelago closed (Dowsett et al. 2016), inhibiting the flow of ocean water from the North Pacific to the Arctic and North Atlantic. Brierley and

Fedorov (2016) modeled the impacts of changes in ocean gateways on various aspects of global climate. They did not find that a closed Bering Strait would have led to large-scale changes in temperature or precipitation over the North Pacific. However, the extent to which a closed Bering Strait impacts temperature, sea level pressure anomalies, and precipitation in the UofT-CCSM4 will be important to our understanding of the mechanisms behind changes in AR behavior observed in this analysis, and warrants further study.

Of relevance to our understanding of this region are recent reconstructions of mid-Pliocene *P–E* using past lake deposits, which suggest a wetter-than-present western United States and imply increased moisture convergence in the region (Ibarra et al., 2018). The simulated hydroclimate in the parts of North America analyzed by Ibarra et al. (2018) shows a mixed signal, with higher *P–E* in some areas and lower *P–E* in other (figures 1e and 1h). Moreover, the UofT-CCSM4 model does not appear to account for the moisture convergence suggested by Ibarra et al. (2018). This points to the importance of further work to understand the mechanisms behind changes in moisture convergence, to identify possible biases in the model, and to constrain aspects of the mid-Piacenzian hydrologic cycle with greater spatial and temporal precision.

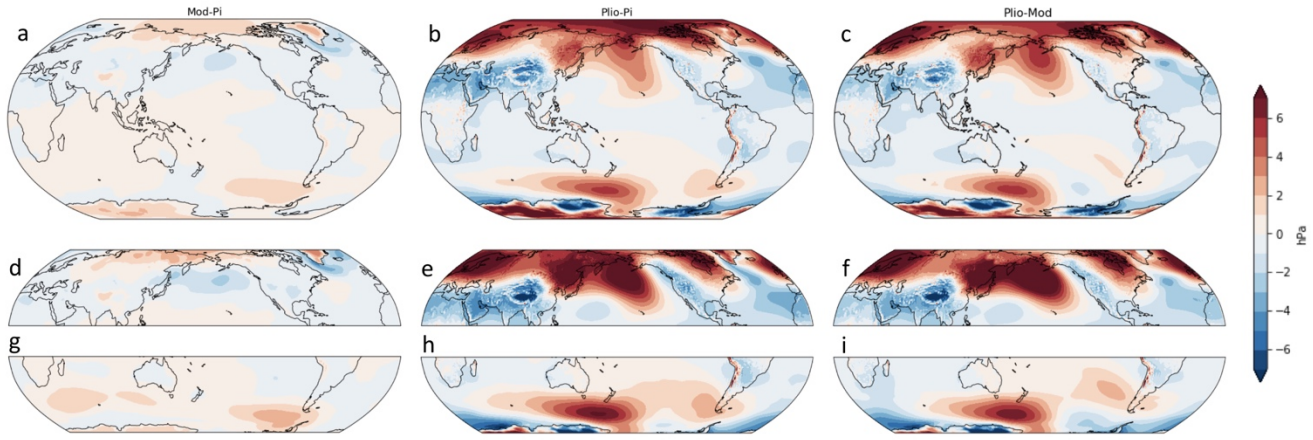

Figure 6. *(a–c) Change in mean sea level pressure anomalies from global mean sea level pressure (hPa), between the modern and preindustrial (a), Pliocene and preindustrial (b), and Pliocene and modern (c). (d–e) Same as (a–c) for NH cool season (November–April). (g–i) Same as (a–c) for SH cool season (May–October).*

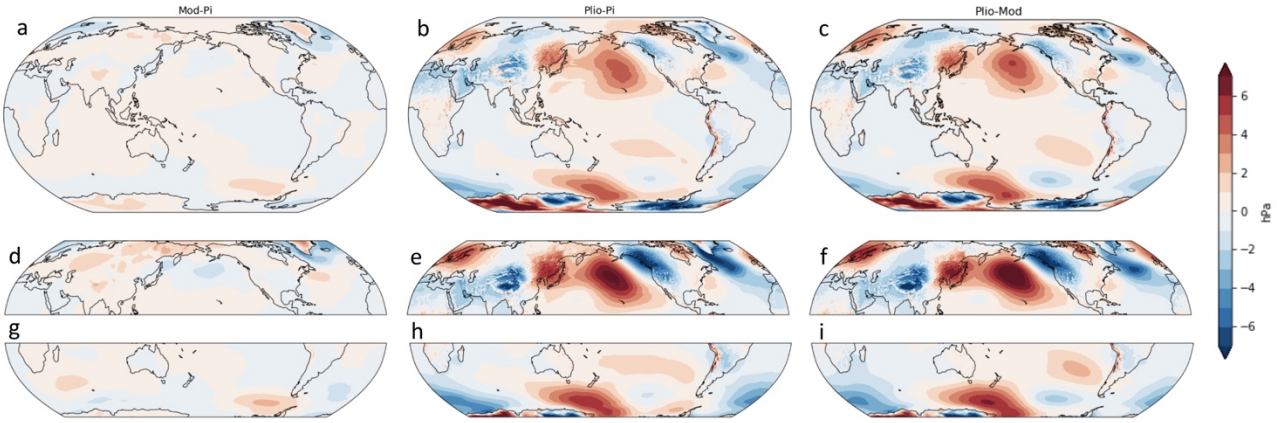

Figure 7. *(a–c) Change in mean sea level pressure anomalies from zonal mean sea level pressure (hPa), between the modern and preindustrial (a), Pliocene and preindustrial (b), and Pliocene and modern (c). (d–e) Same as (a–c) for NH cool season (November–April). (g–i) Same as (a–c) for SH cool season (May–October).*

In the south Pacific, Pliocene cool-season AR precipitation intensifies, shifting southwest-ward compared to the modern control. Pliocene AR precipitation (figures 5b, 5h) intensifies in particular near the southeastern edge of the South Pacific Convergence Zone (SPCZ), an elongated convection zone that stretches diagonally across the south Pacific (Haffke and Magnusdottir, 2013). The SPCZ plays an important role in global atmospheric circulation (Vincent, 1994), and is strongest during the southern hemisphere warm season of November – April (Haffke and Magnusdottir, 2013). Changes in Pliocene AR precipitation suggest a possible intensification of the influence of the SPCZ on the formation of ARs during the southern hemisphere cool season of May – October. This coincides with a poleward shift in midlatitude westerlies and moisture convergence, which can be attributed to the reduced meridional temperature gradient of the Pliocene. Insofar as moisture transport out of the SPCZ determines how ARs form, changes in the SPCZ in warmer climate conditions influence changes in AR behavior, and are worthy of future exploration. A starting point could be a closer analysis of modeled Pliocene precipitation and *P–E* (figure 1e, 1h) showing an expanded "dry zone," a feature identified in Takahashi and Battisti (2007) as the dry region bounded by the SPCZ and coast of South America, and whose expansion suggests a poleward shift of the SPCZ.

The seasonality of AR behavior may also change in the Pliocene, in ways that could have a significant impact on the spatial distribution of AR-related precipitation events. Viale et al. (2018) show with reanalysis, meteorological soundings, and surface precipitation observations that ARs in the region are more frequent during the southern hemisphere winter and spring to the north of 43°S, and are more frequent in the summer and fall to the south of 43°S. A poleward shift in AR precipitation would thus have the effect of shifting winter and spring-time precipitation further south, towards the areas that currently receive more frequent AR precipitation during the summer months. A more detailed seasonal analysis would be useful to explore the relationship between seasonality and spatial shifts in AR precipitation.

Changes in zonal pressure anomalies, depicted in figure 7, show Pliocene pressure anomalies that are lower than the modern and preindustrial over the west Antarctic ice sheet and part of East Antarctica, corresponding with ice-free areas in the PRISM4 reconstruction. Insofar as these signals over Antarctica impact the pattern of pressure anomalies in the south Pacific, these changes would impact patterns of AR precipitation. Furthermore, other topography and land-sea mask changes could impact these shifts in AR behavior. In the Pliocene simulation, dynamical shifts in precipitation interact with increased elevations in the Andes. Higher elevations in the Andes may also have some impact on the SPCZ, due to mechanical responses of atmospheric flow to the Andes, which play a large role in establishing the subtropical dry zone adjacent to the SPCZ (Takahashi and Battisti, 2007). It is also important to consider the impact of the closure of Arctic ocean gateways in the PRISM4 dataset. In the analyses of ocean gateway changes in Brierley and Fedorov (2016), a closed Bering Strait resulted in higher SSTs in the south Pacific, but no large-scale changes in precipitation in that region. As in the North Pacific, the significance of PRISM4 changes in ocean gateways to simulated changes in AR precipitation are difficult to ascertain without further sensitivity analyses using UofT-CCSM4 model output.

Although uncertainties remain regarding the mechanisms behind the response of ARs to Pliocene warming, the simulated changes would bring about significant regional changes in the hydrologic cycle. While recognizing the remaining difficulty of attributing changes in AR precipitation to specific Pliocene boundary features, the following is a preliminary exploration of the impact of shifting ARs on regional precipitation extremes along the Pacific coasts of North America and Chile.

I define the North American region as falling between 32.5°N and 52.5°N, and between 230°E and 245°E. Here, ARs are known to contribute to water resources, heavy precipitation, snowpack variability, and flooding (Payne and Magnusdottir, 2014; Ralph et al., 2006; Dettinger et al., 2011; Rutz and Steenburgh, 2012; Guan et al., 2010). In the preindustrial control, 31.7% of overall cool-season precipitation in this region is attributable to ARs. In the modern simulation, that fraction increases to 36.9%, but in the Pliocene simulation decreases to 26.8%. For extreme precipitation events (exceeding the 99th percentile), the contribution of AR precipitation to the total follows a similar pattern: from 53.6% in the preindustrial, it increases to 57.0% in the modern but decreases to 46.6% in the Pliocene control. This appears to be a direct effect of the overall decrease in AR precipitation in the region as previously discussed and as shown in figure 4.

Figure 8 demonstrates changes in the frequency of AR extreme precipitation, defined as AR precipitation events exceeding the 99th percentile of the preindustrial control, along the North American Coast. It is evident that while AR extreme precipitation increases in the modern, it does not follow the monotonic increase in the Pliocene simulation that one might expect if considering purely thermodynamic effects. Rather, AR extreme precipitation in the Pliocene decreases in most parts of the region, with some positive anomalies that appear in part related to changes in topographic changes.

Further implications of changing AR behavior in this region are evident in figure 9. Figures 9a and 9b depict the intensity of extreme precipitation and their rates of increase for the modern and Pliocene simulations, this time focusing only on the specified North American Coastal region. The intensity of 99th, 99.9th, and 99.97th percentile extremes increases in the modern control but decreases in the Pliocene. Similarly, figures 9c and 9d respectively depict the frequency of extreme precipitation events and their rates of change. The frequency of extreme events increases monotonically in the modern. In the Pliocene, however, only the most extreme (99.9th and 99.97th percentile) events occur more often than in the preindustrial control, and even in those cases they occur less often than in the modern simulation. Given that ARs contribute such a substantial volume of extreme precipitation in this region, it becomes evident that the simulated shift of AR precipitation away from the North American coast strongly influences Pliocene levels of extreme precipitation in this region.

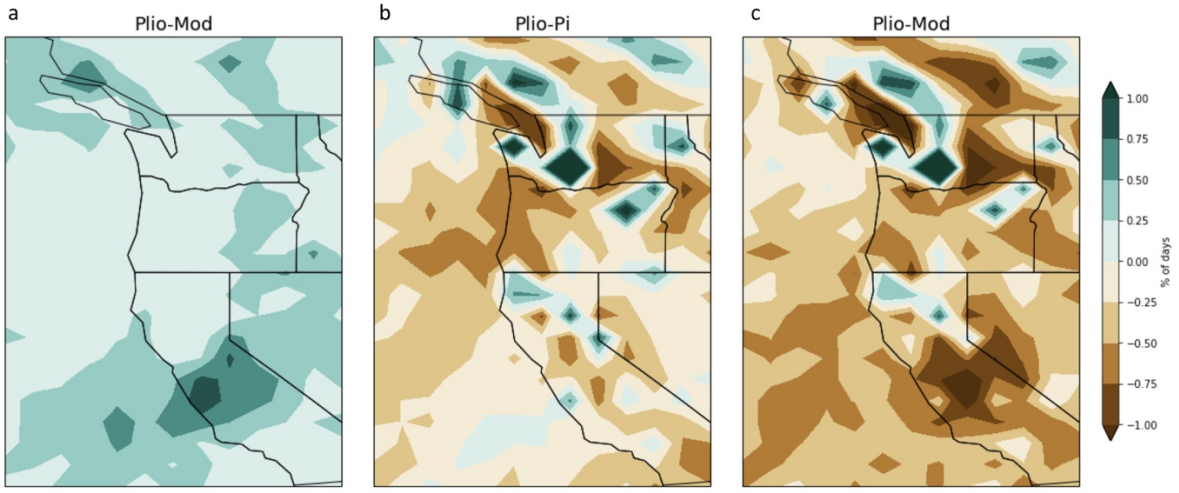

Figure 8. *Change in frequency of AR extreme precipitation in the NH cool season (November – April), defined as AR precipitation exceeding the 99th percentile of mean cool-season precipitation in the preindustrial for each grid point. Differences between modern and preindustrial (a), Pliocene and preindustrial (b), and Pliocene and modern (c) are shown.*

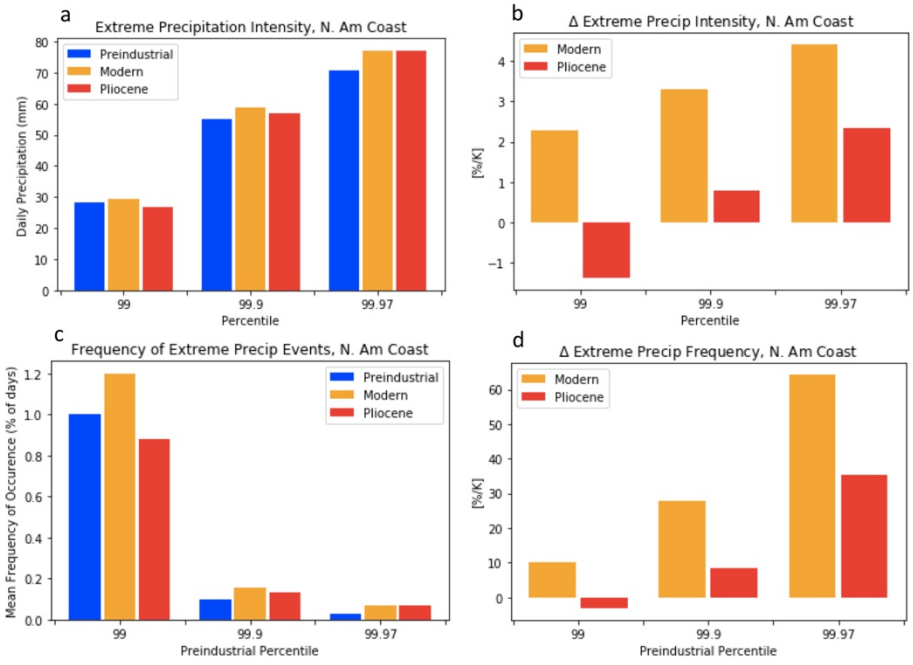

Figure 9. *Same as figure 2, but for the North American coastal region depicted in figure 8.*

ARs are also known to play an important role in precipitation along the coast of Chile (Viale et al. 2018). In this study, I define the South American region as falling between 38°S and 50°S, latitudes where ARs are most likely to occur in the present day (Viale et al. 2018), and between 280°E and 300°E. In this region, ARs account for 24.7% of overall cool-season (May – October) precipitation, a fraction that increases to 26.0% in the modern and 33.3% in the Pliocene. The AR contribution to extreme precipitation is 51.6% in the preindustrial, 46.3% in the modern, and 52.5% in the Pliocene. While AR precipitation and AR extreme precipitation both increase, so do non-AR precipitation and extreme precipitation, so the changing fractions of AR precipitation reflect changes in the relative rates of increase of AR (extreme) precipitation and overall (extreme) precipitation.

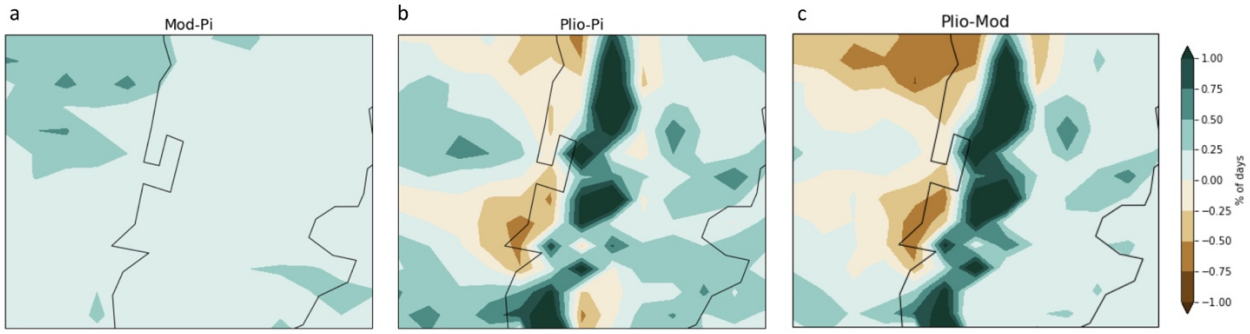

Figure 10. *Change in frequency of AR extreme precipitation in the NH cool season (November – April), defined as AR precipitation exceeding the 99th percentile of mean cool-season precipitation in the preindustrial for each grid point. Differences between modern and preindustrial (a), Pliocene and preindustrial (b), and Pliocene and modern (c) are shown.*

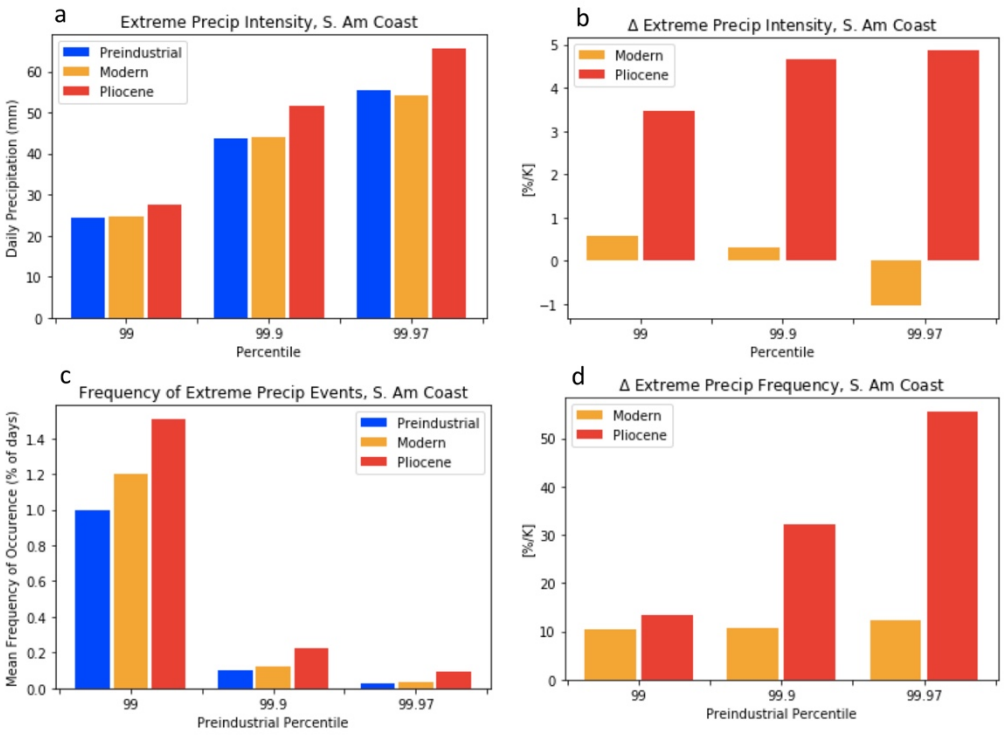

Figure 11. *Same as figure 2, but for the South American coastal region depicted in figure 9.*

Unlike the North American coast, AR precipitation increases throughout the entire area of the South American coast. Figure 10 depicts increases in AR extreme precipitation in the modern (10a), and further increases in the Pliocene (10b) with regional variation that might be explained by changes in topography. Figures 11a and 11b demonstrate increases in the intensity of 99th, 99.9th, and 99.97th Pliocene precipitation in this region, at rates greater than the modern (in fact, the intensity of 99.97th percentile modern decreases compared to the preindustrial). Figures 11c and 11d show monotonic increases in the frequency of extreme precipitation events in the modern and in the Pliocene, with Pliocene frequencies increasing at a faster rate with warming especially for the most extreme events.

These two regions demonstrate a clear tension between the expected thermodynamic effects of warming (in the sense of Katz and Brown, 1992) and dynamical changes in moisture convergence. Moreover, they exemplify how these factors can influence different levels of precipitation (e.g. mean, extreme, very extreme) in different ways. Because the hydrologic cycle

in these areas is known to be heavily determined by AR precipitation, these results motivate further inquiry into the dynamics of changes in the behavior of atmospheric rivers.

5. Summary and Discussion

This study used the UofT-CCSM4 model of mid-Piacenzian climate to analyze simulated changes in the hydrologic cycle. Globally, the frequency and intensity of extreme precipitation increased in comparison to the preindustrial and modern conditions, with the largest relative changes occurring for the most extreme heavy precipitation events. Despite this overall increase, there were large regional differences in how the intensity and frequency of precipitation extremes changed in the Pliocene. ARs are one feature of the atmosphere driving these regional differences.

The model simulation of Pliocene climate revealed dynamical changes in the behavior of atmospheric rivers that heavily influenced regional levels of precipitation, especially extreme precipitation. In both the north Pacific and south Pacific, the Pliocene climate experienced changes in AR precipitation that were substantially different from the changes observed in the modern simulation. In the coastal regions affected by AR precipitation in these areas, the effects of changes in AR behavior were substantially different. These results highlight how changes in the hydrologic cycle affect different regions in very different ways. They also reaffirm the role of ARs as important climatological features impacting past and future climate, whose changing behavior as the climate warms has not been fully constrained.

While this analysis was conducted using one model of mid-Piacenzian climate, other models using PRISM4/PlioMIP2 boundary conditions reproduce values of global annual mean precipitation increases (ΔPrecip) ranging from 0.07 to 0.37 mm/day, with an ensemble mean ΔPrecip of 0.17 mm/day (Haywood et al., in review). Models concur on broad spatial features such as increased precipitation in the subtropics and a poleward shift of higher latitude precipitation (Haywood et al., in review), but vary in significant ways. Thus, future studies might analyze elements of Pliocene hydrologic cycle using output from different models, and compare results to those described here.

Moreover, this analysis was limited in scope but suggests future areas of study that would improve our understanding of the dynamics of ARs in this model and others. More precise seasonal analyses of AR behavior would lend more detail to the broad patterns identified, and

analyses of the impact of AR behavior on other regions would place the impacts of ARs on the regions studied here in broader context. This paper suggested broad mechanisms that might explain identified changes in AR behavior. In addition to increases in global mean temperature, ARs are affected by the reduced Pliocene temperature gradients that result from the polar amplification of warming. However, the relative contributions of this factor and others remain unclear, as Pliocene differences in orography, bathymetry, and continental configuration also influence the hydrologic cycle. To better understand these dynamics, improvements in Pliocene modelling will be instrumental. Improved simulation of poorly constrained elements such as cloud feedbacks (Burls and Fedorov, 2014) would more completely explain the mechanisms behind broad features of the Pliocene climate.

While regional effects of changes in AR behavior are drastic, it is unclear whether these modeled changes manifested in the same way during the mid-Piacenzian. The verification of modeled changes in the hydrologic cycle is limited by the types of paleoenvironmental reconstructions available, the amount of such information available, and the often different resolutions of data from proxy reconstructions and paleoclimate models. Reconstructions of precipitation patterns are less comprehensive than reconstructions of pCO_2 and sea surface temperature. Moreover, the geographical scope of available proxy reconstructions to inform us about the Pliocene hydrologic cycle is limited. Thus, fully understanding the hydrologic cycle of the Pliocene will require further advancements in modelling and paleoenvironmental reconstruction.

The mid-Piacenzian has been discussed as the best historical analog for the type of warmer world toward which our climate is evolving. Its promise lies especially in its potential to reveal longer-term processes that are difficult to constrain in models of future warming scenarios. The impact of warming on the frequency, intensity, and regional distribution of precipitation extremes is one such feature—highly relevant to society, but presently difficult to describe. Models of mid-Piacenzian climate might provide an additional tool with which to study this urgent question, and/or shed light on key differences between hydrologic cycles of past and future warm states. These possibilities justify further work in this area.

6. Acknowledgements

I'd like to sincerely thank Juan Lora for his thoughtful guidance, mentorship, and support in all stages of this project. I'm grateful to Deepak Chandan and Richard Peltier for sharing their model output with me. Thanks to Kaylea Nelson to answering many of my questions, and to the Yale Center for Research Computing for maintaining the Grace computing cluster. Thanks also to Alexey Fedorov for his time as a second reader, and to Mary-Louise Timmermans for introducing me to the major my first year.

Finally, I'd like to acknowledge my communities in Timothy Dwight College, St. Anthony Hall, and the Yale Gymnastics Team for being steady sources of confidence and love.

7. References

Alexander, L. V. Global observed long-term changes in temperature and precipitation extremes: A review of progress and limitations in IPCC assessments and beyond. *Weather and Climate Extremes* 11, 4–16 (2016).

Badger, M. P. S., Schmidt, D. N., Mackensen, A. & Pancost, R. D. High-resolution alkenone palaeobarometry indicates relatively stable pCO2 during the Pliocene (3.3–2.8 Ma). *Philosophical Transactions of the Royal Society A: Mathematical, Physical and Engineering Sciences* 371, 20130094 (2013).

Bartoli, G., Hönisch, B. & Zeebe, R. E. Atmospheric CO2 decline during the Pliocene intensification of Northern Hemisphere glaciations. *Paleoceanography* 26, (2011).

Blamey, R. C., Ramos, A. M., Trigo, R. M., Tomé, R. & Reason, C. J. C. The Influence of Atmospheric Rivers over the South Atlantic on Winter Rainfall in South Africa. *J. Hydrometeor.* 19, 127–142 (2017).

Brierley, C. M. & Fedorov, A. V. Comparing the impacts of Miocene–Pliocene changes in inter-ocean gateways on climate: Central American Seaway, Bering Strait, and Indonesia. *Earth and Planetary Science Letters* 444, 116–130 (2016).

Burls, N. J. & Fedorov, A. V. Simulating Pliocene warmth and a permanent El Niño-like state: The role of cloud albedo. *Paleoceanography* 29, 893–910 (2014).

Burls, N. J. & Fedorov, A. V. Wetter subtropics in a warmer world: Contrasting past and future hydrological cycles. *PNAS* 114, 12888–12893 (2017).

Chandan, D. & Peltier, W. R. Regional and global climate for the mid-Pliocene using the University of Toronto version of CCSM4 and PlioMIP2 boundary conditions. *Climate of the Past* 13, 919–942 (2017).

Chandan, D. & Peltier, W. R. On the mechanisms of warming the mid-Pliocene and the inference of a hierarchy of climate sensitivities with relevance to the understanding of climate futures. *Climate of the Past* 14, 825–856 (2018).

Chou, C., Neelin, J. D., Chen, C.-A. & Tu, J.-Y. Evaluating the "Rich-Get-Richer" Mechanism in Tropical Precipitation Change under Global Warming. *J. Climate* 22, 1982–2005 (2009).

Corvec, S. & Fletcher, C. G. Changes to the tropical circulation in the mid-Pliocene and their implications for future climate. *Climate of the Past* 13, 135–147 (2017).

Dettinger, M. D., Ralph, F. M., Das, T., Neiman, P. J. & Cayan, D. R. Atmospheric Rivers, Floods and the Water Resources of California. *Water* 3, 445–478 (2011).

Donat, M. G., Lowry, A. L., Alexander, L. V., O'Gorman, P. A. & Maher, N. More extreme precipitation in the world's dry and wet regions. *Nature Climate Change* 6, 508–513 (2016).

Dowsett, H. *et al.* The PRISM4 (mid-Piacenzian) paleoenvironmental reconstruction. *Climate of the Past* 12, 1519–1538 (2016).

Dutton, A. *et al.* Sea-level rise due to polar ice-sheet mass loss during past warm periods. *Science* 349, aaa4019–aaa4019 (2015).

Fedorov, A. V., Brierley, C. M. & Emanuel, K. Tropical cyclones and permanent El Niño in the early Pliocene epoch. *Nature* 463, 1066–1070 (2010).

Fischer, E. M. & Knutti, R. Observed heavy precipitation increase confirms theory and early models. *Nature Climate Change* 6, 986–991 (2016).

Grant, G. R. *et al.* The amplitude and origin of sea-level variability during the Pliocene epoch. *Nature* 574, 237–241 (2019).

Guan, B., Molotch, N. P., Waliser, D. E., Fetzer, E. J. & Neiman, P. J. Extreme snowfall events linked to atmospheric rivers and surface air temperature via satellite measurements. *Geophysical Research Letters* 37, (2010).

Haffke, C. & Magnusdottir, G. The South Pacific Convergence Zone in three decades of satellite images: SPCZ three decades of satellite images. *Journal of Geophysical Research: Atmospheres* 118, 10,839-10,849 (2013).

Haywood, A. M. *et al.* Large-scale features of Pliocene climate: results from the Pliocene Model Intercomparison Project. *Climate of the Past* 9, 191–209 (2013).

Haywood, A. M., Dowsett, H. J. & Dolan, A. M. Integrating geological archives and climate models for the mid-Pliocene warm period. *Nature Communications* 7, (2016).

Haywood, A. M., *et al.* A return to large-scale features of Pliocene climate: the Pliocene Model Intercomparison Project Phase 2. (in review).

Held, I. M. & Soden, B. J. Robust Responses of the Hydrological Cycle to Global Warming. *J. Climate* 19, 5686–5699 (2006).

Horikawa, K. *et al.* Pliocene cooling enhanced by flow of low-salinity Bering Sea water to the Arctic Ocean. *Nature Communications* 6, 1–9 (2015).

Ibarra, D. E. *et al.* Warm and cold wet states in the western United States during the Pliocene–Pleistocene. *Geology* 46, 355–358 (2018).

IPCC: Climate Change 2013: The Physical Science Basis. Contribution of Working Group I to the Fifth Assessment Report of the Intergovernmental Panel on Climate Change. Cambridge University Press, Cambridge, United Kingdom and New York, NY, USA. 2013.

Katz, R. W. & Brown, B. G. Extreme events in a changing climate: Variability is more important than averages. *Climatic Change* 21, 289–302 (1992).

Kim, H.-M., Zhou, Y. & Alexander, M. A. Changes in atmospheric rivers and moisture transport over the Northeast Pacific and western North America in response to ENSO diversity. *Clim Dyn* 52, 7375–7388 (2019).

Kim, H.-J. & An, S.-I. Impact of North Atlantic Freshwater Forcing on the Pacific Meridional Overturning Circulation under Glacial and Interglacial Conditions. *J. Climate* 32, 4641–4659 (2019).

Lavers, D. A. *et al.* Future changes in atmospheric rivers and their implications for winter flooding in Britain. *Environ. Res. Lett.* 8, 034010 (2013).

Li, X. *et al.* Mid-Pliocene westerlies from PlioMIP simulations. *Advances in Atmospheric Sciences* 32, 909–923 (2015).

Lora, J. M. Components and Mechanisms of Hydrologic Cycle Changes over North America at the Last Glacial Maximum. *Journal of Climate* 31, 7035–7051 (2018).

Martínez-Botí, M. A. *et al.* Plio-Pleistocene climate sensitivity evaluated using high-resolution CO 2 records. *Nature* 518, 49–54 (2015).

Min, S.-K., Zhang, X., Zwiers, F. W. & Hegerl, G. C. Human contribution to more-intense precipitation extremes. *Nature* 470, 378–381 (2011).

Myhre, G. *et al.* Frequency of extreme precipitation increases extensively with event rareness under global warming. *Scientific Reports* 9, (2019).

Newman, M., Kiladis, G. N., Weickmann, K. M., Ralph, F. M. & Sardeshmukh, P. D. Relative Contributions of Synoptic and Low-Frequency Eddies to Time-Mean Atmospheric Moisture Transport, Including the Role of Atmospheric Rivers. *J. Climate* 25, 7341–7361 (2012).

O'Gorman, P. A. & Schneider, T. The physical basis for increases in precipitation extremes in simulations of 21st-century climate change. *Proceedings of the National Academy of Sciences* 106, 14773–14777 (2009).

O'Gorman, P. A. Precipitation Extremes Under Climate Change. *Curr Clim Change Rep* 1, 49–59 (2015).

Otto-Bliesner, B. L. *et al.* Amplified North Atlantic warming in the late Pliocene by changes in Arctic gateways: Arctic Gateways and Pliocene Climate. *Geophysical Research Letters* 44, 957–964 (2017).

Pagani, M. Broken tropical thermostats. *Nature Geoscience* 7, 555–556 (2014).

Payne, A. E. & Magnusdottir, G. Dynamics of Landfalling Atmospheric Rivers over the North Pacific in 30 Years of MERRA Reanalysis. *Journal of Climate* 27, 7133–7150 (2014).

Pendergrass, A. G. & Hartmann, D. L. Changes in the Distribution of Rain Frequency and Intensity in Response to Global Warming. *Journal of Climate* 27, 8372–8383 (2014).

Ralph, F. M. & Dettinger, M. D. Storms, floods, and the science of atmospheric rivers. *Eos, Transactions American Geophysical Union* 92, 265–266 (2011).

Ralph, F. M. *et al.* Atmospheric Rivers Emerge as a Global Science and Applications Focus. *Bulletin of the American Meteorological Society* 98, 1969–1973 (2017).

Ralph, F. Martin, et al. "Flooding on California's Russian River: Role of atmospheric rivers." *Geophysical Research Letters* 33.13 (2006).

Rutz, J. J. & Steenburgh, W. J. Quantifying the role of atmospheric rivers in the interior western United States. *Atmospheric Science Letters* 13, 257–261 (2012).

Rutz, J. J., Steenburgh, W. J. & Ralph, F. M. Climatological Characteristics of Atmospheric Rivers and Their Inland Penetration over the Western United States. *Mon. Wea. Rev.* 142, 905–921 (2013).

Salzmann, U., Haywood, A. M., Lunt, D. J., Valdes, P. J. & Hill, D. J. A new global biome reconstruction and data-model comparison for the Middle Pliocene. *Global Ecology and Biogeography* 17, 432–447 (2008).

Seager, R., Naik, N. & Vecchi, G. A. Thermodynamic and Dynamic Mechanisms for Large-Scale Changes in the Hydrological Cycle in Response to Global Warming. *Journal of Climate* 23, 4651–4668 (2010).

Skinner, C.B., Lora, J.M., Payne, A.E., & Poulsen, C.J. Atmospheric river changes shaped mid-latitude hydroclimate since the mid-Holocene. Earth and Planetary Science Letters, accepted.

Soden, B. J. & Held, I. M. An Assessment of Climate Feedbacks in Coupled Ocean–Atmosphere Models. *Journal of Climate* 19, 3354–3360 (2006).

Takahashi, K. & Battisti, D. S. Processes Controlling the Mean Tropical Pacific Precipitation Pattern. Part II: The SPCZ and the Southeast Pacific Dry Zone. *J. Climate* 20, 5696–5706 (2007).

Trenberth, K. Changes in precipitation with climate change. *Climate Research* 47, 123–138 (2011).

Tsing, A. L., Mathews, A. S. & Bubandt, N. Patchy Anthropocene: Landscape Structure, Multispecies History, and the Retooling of Anthropology: An Introduction to Supplement 20. *Current Anthropology* 60, S186–S197 (2019).

Vallis, G. K., Zurita-Gotor, P., Cairns, C. & Kidston, J. Response of the large-scale structure of the atmosphere to global warming. *Quarterly Journal of the Royal Meteorological Society* 141, 1479–1501 (2015).

Vecchi, G. A. & Soden, B. J. Global Warming and the Weakening of the Tropical Circulation. *J. Climate* 20, 4316–4340 (2007).

Viale, M. & Nuñez, M. N. Climatology of Winter Orographic Precipitation over the Subtropical Central Andes and Associated Synoptic and Regional Characteristics. *J. Hydrometeor.* 12, 481–507 (2010).

Viale, M., Valenzuela, R., Garreaud, R. D. & Ralph, F. M. Impacts of Atmospheric Rivers on Precipitation in Southern South America. *Journal of Hydrometeorology* 19, 1671–1687 (2018).

Vincent, D. G. The South Pacific Convergence Zone (SPCZ): A Review. *Mon. Wea. Rev.* 122, 1949–1970 (1994).

Wara, M. W., Ravelo, A. C. & Delaney, M. L. Permanent El Nino-Like Conditions During the Pliocene Warm Period. *Science* 309, 758–761 (2005).

Zhang, X., Wan, H., Zwiers, F. W., Hegerl, G. C. & Min, S.-K. Attributing intensification of precipitation extremes to human influence. *Geophysical Research Letters* 40, 5252–5257 (2013).

Zhu, Y. & Newell, R. E. A Proposed Algorithm for Moisture Fluxes from Atmospheric Rivers. *Mon. Wea. Rev.* 126, 725–735 (1998).

8. Appendix

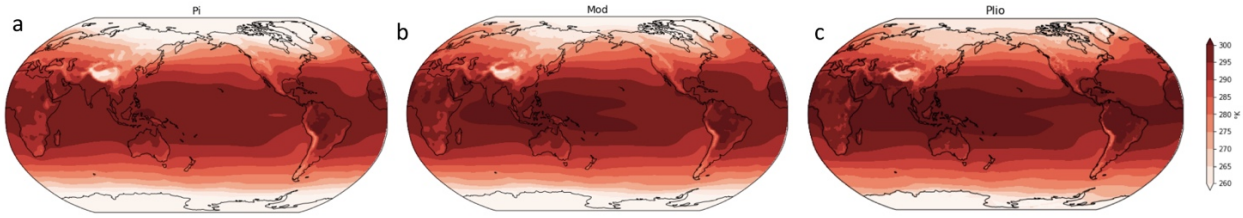

Appendix 1. *Mean surface temperature (°K) in the preindustrial (a), modern (b), and Pliocene (c).*

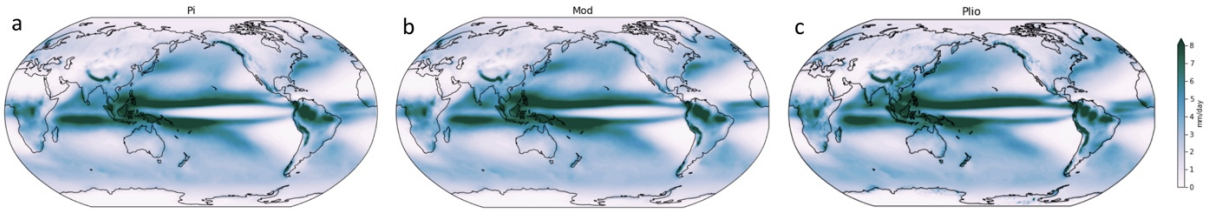

Appendix 2. *Absolute precipitation (mm/day) in the preindustrial (a), modern (b), and Pliocene (c).*

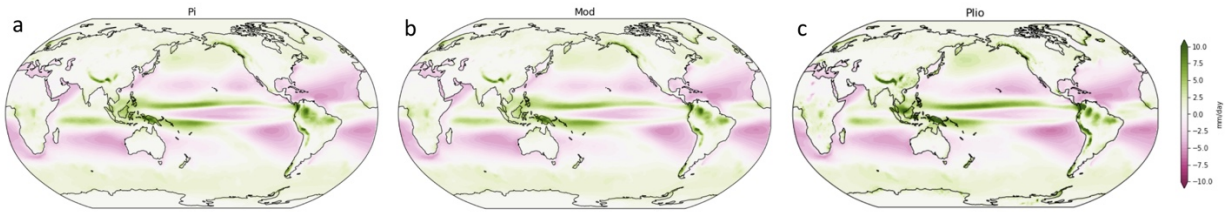

Appendix 3. *Absolute P–E (mm/day) in the preindustrial (a), modern (b), and Pliocene (c).*

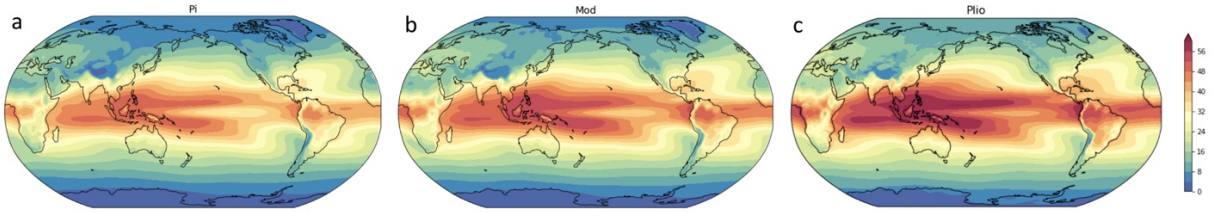

Appendix 4. *Mean integrated water vapor ($kgm^{-1}s^{-1}$) for preindustrial (a), modern (b), and Pliocene (c).*

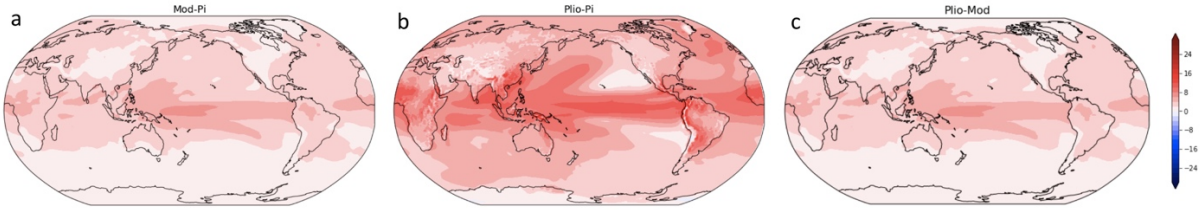

Appendix 5. *Change in mean integrated water vapor (kg $m^{-1}s^{-1}$) for modern-preindustrial (a), Pliocene-preindustrial (b), and Pliocene-Modern (c).*

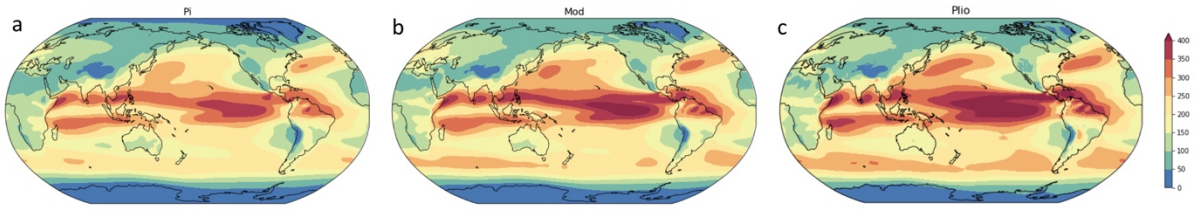

Appendix 6. *Mean integrated vapor transport (kg $m^{-1}s^{-1}$) for preindustrial (a), modern (b), and Pliocene (c).*

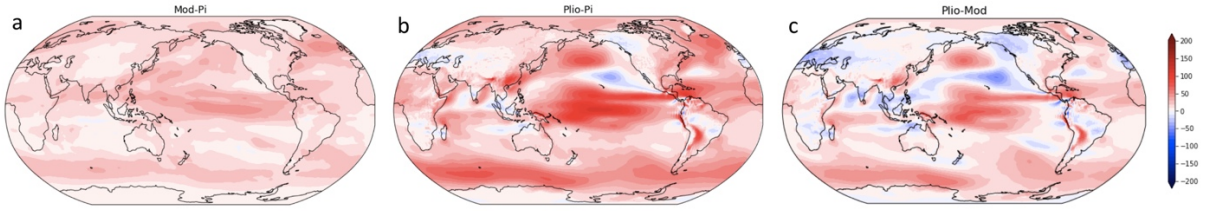

Appendix 7. *Change in mean integrated vapor transport (kg $m^{-1}s^{-1}$) for modern-preindustrial (a), Pliocene-preindustrial (b), and Pliocene-Modern (c).*

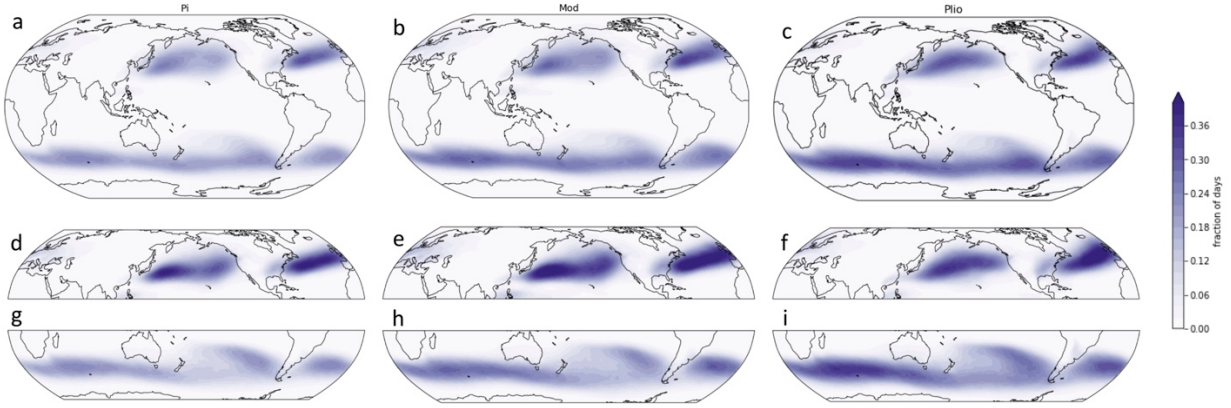

Appendix 8. *(a–c) AR frequency (fraction of days), for preindustrial (a), modern (b), and Pliocene (c). (d–f) Same as (a–c) for NH cool season (November–April). (g–i) Same as (a–c) for SH cool season (May–October).*

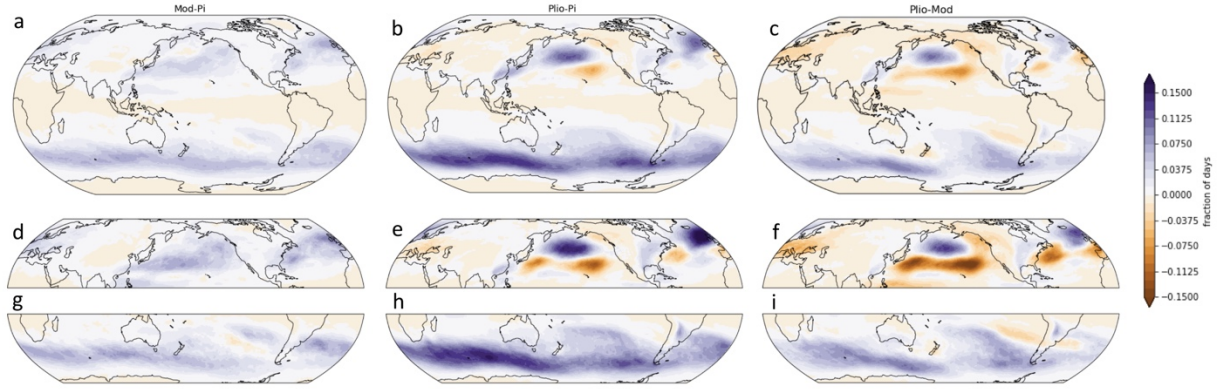

Appendix 9. *(a–c) Change in AR frequency (fraction of days) for modern-preindustrial, Pliocene-preindustrial, and Pliocene-modern. (d–f) Same as (a–c) for NH cool season (November–April). (g–h) Same as (a–c) for SH cool season (May–October).*

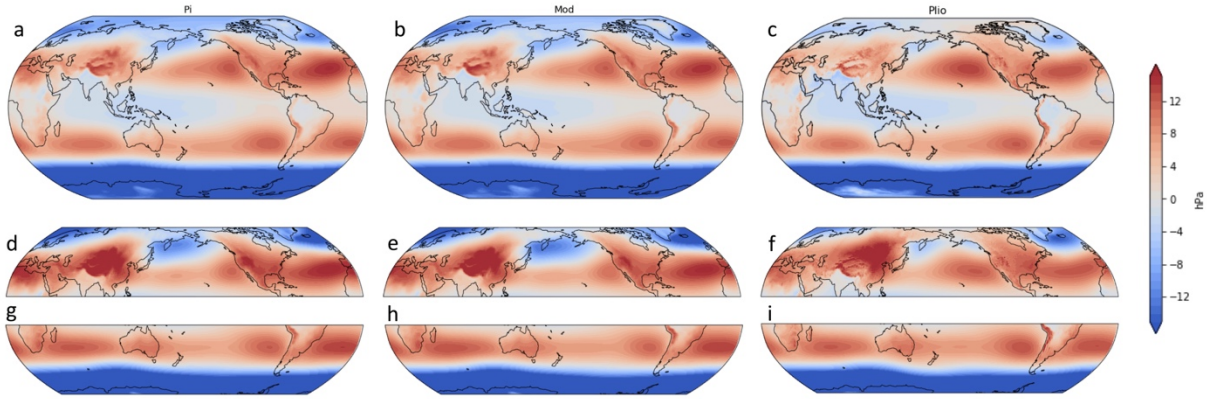

Appendix 10. *(a–c) Sea level pressure anomalies (hPa) for modern-preindustrial, Pliocene-preindustrial, and Pliocene-modern. (d–f) Same as (a–c) for NH cool season (November–April). (g–h) Same as (a–c) for SH cool season (May–October).*

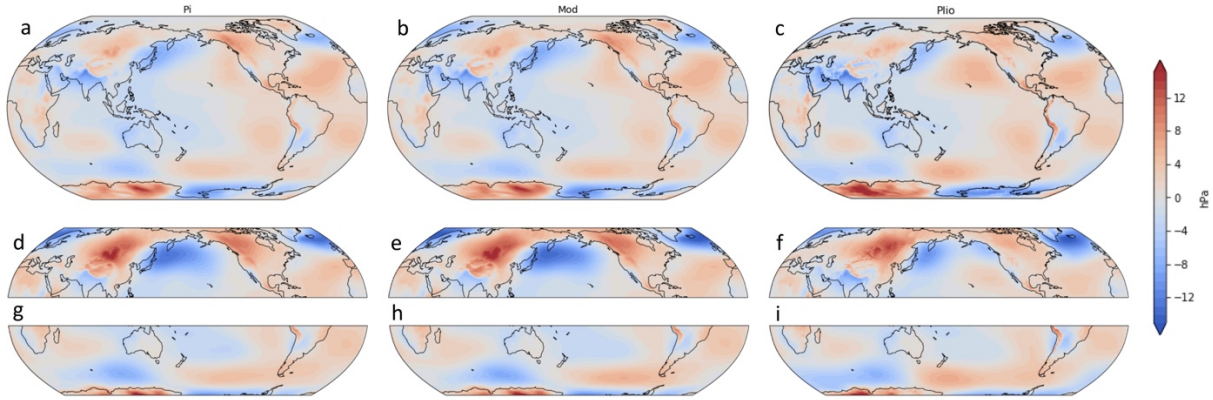

Appendix 10. *(a–c) Zonal sea level pressure anomalies (hPa) for modern-preindustrial, Pliocene-preindustrial, and Pliocene-modern. (d–f) Same as (a–c) for NH cool season (November–April). (g–h) Same as (a–c) for SH cool season (May–October).*